https://doi.org/10.5194/egusphere-2026-2155
Preprint. Discussion started: 30 April 2026

Long-Lived High-Frequency Gravity Waves over the Southern Ocean and the East Antarctic coastline and Their Influence on Cloud Properties

Wenyue Wang[1], Adrian J. McDonald[1,2], Simon Alexander[3,4], and Klemens Hocke[5,6]

[1]School of Physical and Chemical Sciences, University of Canterbury, Christchurch, Aotearoa / New Zealand
[2]Gateway Antarctica, University of Canterbury, Christchurch, Aotearoa / New Zealand
[3]Australian Antarctic Division, Hobart, Australia
[4]Australian Antarctic Program Partnership, Institute for Marine and Antarctic Studies, University of Tasmania, Hobart, Australia
[5]Institute of Applied Physics, University of Bern, Bern, Switzerland
[6]Oeschger Centre for Climate Change Research, University of Bern, Bern, Switzerland

Correspondence: Wenyue Wang (wenyue.wang@canterbury.ac.nz)

Abstract. The Southern Ocean near the East Antarctic coast is a dynamic source of gravity waves, yet long-lived high-frequency gravity waves (HFGWs) remain poorly documented. Using four months of ship-based remote sensing and in-situ observations, this study analyses the characteristics of HFGWs and their influence on cloud properties near three Antarctic coastal stations (Davis, Casey, and Mawson) through statistical analyses and detailed case studies. Doppler vertical velocity oscillations are observed in clouds with tops around 8 km, with amplitudes mainly near 0.02 m s^{-1}. These clouds are primarily ice. Based on radiosonde ascent rates and Richardson number analysis, the oscillations are identified as gravity waves. The observed gravity waves typically exhibit periods close to the buoyancy period (about 10 minutes) and horizontal wavelengths of 3 km, and can be tracked for up to 48 hours (approximately 220–320 wave cycles). Approximately 46% of valid Doppler velocity data within clouds exhibited high-frequency oscillations associated with HFGWs. These occurrences covered 91% of cloudy days, indicating that such waves are ubiquitous. Periodic variations in reflectivity further suggest that these waves modulate cloud properties. Potential sources of the HFGWs are investigated using air-mass trajectories, ERA5 reanalysis, and MODIS observations. The waves are most likely generated by multiple sources including cyclonic activity, katabatic winds, and jet-related synoptic forcing. In some cases a thermal duct, together with a concurrent low-frequency gravity wave background, provides a multiscale environment that likely supports the HFGWs long-lived nature.

1 Introduction

Atmospheric gravity waves (GWs) are ubiquitous in the atmosphere and influence the dynamics of all atmospheric layers. By propagating upward from lower-atmospheric sources, GWs transfer energy and momentum into the middle and upper atmosphere, thereby exerting a strong influence on the large-scale circulation (e.g., Alexander et al., 2016; Franco-Diaz et al., 2024). Under certain conditions, gravity wave instabilities can generate turbulence, which may pose hazards to aviation safety

https://doi.org/10.5194/egusphere-2026-2155
Preprint. Discussion started: 30 April 2026

and infrastructure (Hines, 1988). In addition, GWs can enhance convective activity and modulate tropopause height, thereby promoting the transport of ozone with relatively low concentrations and potentially reducing ozone levels (Kidston et al., 2015; Chang et al., 2024). Gravity waves are generated by a variety of sources, including orographic forcing, convection, frontal systems, jet streams, and regions of strong wind shear (Geldenhuys et al., 2021; Plougonven and Zhang, 2014; McDonald et al., 2010). With abundant wave sources and favorable propagation conditions, the conditions over the Southern Ocean, particularly in the vicinity of the Antarctic coastline, are considered one of the most active regions for GWs globally (Plougonven et al., 2013; Baumgaertner and McDonald, 2007; McDonald, 2012; Murphy et al., 2014). Nevertheless, the sources and properties of GWs over the Southern Ocean remain less well documented than those at mid- and low-latitudes. In East Antarctica, synoptic winds or katabatic winds interacting with mountain terrain or coastal ice ridgelines can generate large scale orographic gravity waves (Watanabe et al., 2006; Vignon et al., 2020), while non-orographic gravity waves are commonly associated with nearshore cyclones and unbalanced flows related to jet-front adjustments (Alexander et al., 2017, 2016).

High-frequency gravity waves (HFGWs) have small spatial and temporal scales, with typical periods ranging from several to tens of minutes and horizontal wavelengths of a few to several tens of kilometres (Alexander et al., 1995; Cao and Liu, 2022). Observational evidence of such waves has been reported using coherent Doppler lidar measurements, which revealed HFGWs with periods of 10–30 minutes at around 2 km altitude within the atmospheric boundary layer (Jia et al., 2019). In that study, persistent waves lasting for about 10 hours (exceeding 20 wave cycles) were detected, highlighting the potential for HFGWs to maintain long lifetimes under favorable atmospheric conditions. Dynamically, HFGWs are characterized by frequencies approaching the Brunt–Väisälä frequency (buoyancy frequency) and a strong dependence on stable stratification. When trapped within a waveguide, HFGWs can experience suppressed vertical propagation and predominantly transport energy horizontally, allowing them to persist over extended regions and interact efficiently with clouds (Jia et al., 2019). Previous studies have demonstrated that such interactions can substantially influence cloud microphysical processes (Schoeberl et al., 2016; Alexander et al., 2000); for instance, Jensen et al. (2016) showed that HFGW-induced rapid cooling can promote homogeneous ice nucleation in cold cirrus clouds, leading to enhanced ice crystal concentrations. Despite their importance, the relatively coarse spatial and temporal resolution of most weather and climate models severely limit their ability to accurately represent HFGWs. As a result, such waves are often unresolved and may be poorly parameterized, which can lead to biases in simulated cloud structures. This highlights the need to improve our understanding of HFGWs, their sources, occurrence, and influence on clouds.

Numerous techniques have been employed to study GWs over East Antarctica (Vignon et al., 2020; Alexander et al., 2017; Watanabe et al., 2006; Alexander and Murphy, 2015; Plougonven et al., 2013). Among these, satellite products have been particularly valuable for capturing the large-scale spatial distribution of atmospheric GWs. These observations have also been useful in investigating their role in the formation and distribution of Antarctic polar stratospheric clouds (PSCs) (McDonald et al., 2009; Wu and Jiang, 2002; Alexander et al., 2011). Despite their excellent spatial coverage, limitations in temporal and vertical resolution reduce the ability of satellite products to resolve HFGWs. In contrast, the ground-based VHF wind profiler radar at Syowa and Davis, Antarctica, provide high-temporal-resolution wind measurements and are well suited for quantifying HFGW activity. These VHF radars retrieve zonal, meridional, and vertical velocity profiles from approximately 2 to 15

https://doi.org/10.5194/egusphere-2026-2155
Preprint. Discussion started: 30 April 2026

km altitude at 8-minute temporal resolution (Alexander and Murphy, 2015; Tomikawa et al., 2015). However, as single-site instruments, they offer only a localized perspective, which limits their representativeness and hampers large-scale statistical analyses over East Antarctica. Recent ship-based observational campaigns focused on understanding the limitations in simulating clouds over the Southern Ocean (Alexander et al., 2021), provide valuable data that may also help alleviate limitations in HFGW observations. The Measurements of Aerosols, Radiation, and Clouds over the Southern Ocean (MARCUS) campaign was conducted from October 2017 to March 2018, deploying state-of-the-art, continuous, high-temporal-resolution remote sensing and in-situ instruments onboard the *RSV Aurora Australis* icebreaker (McFarquhar et al., 2021). By traversing between Hobart, Australia, and the Australian East Antarctic stations, MARCUS sampled coastal, oceanic, and Antarctic marginal regions, effectively bridging the observational gap between fixed ground stations and satellite measurements.

Many previous studies have shown that Doppler velocity observations from radars and lidars are effective in observing gravity-wave signatures. For example, Lamer et al. (2021) employed a Ka-band scanning polarimetric radar and identified gravity wave features with periods of 5–6 minutes in Doppler velocity throughout the entire hydrometeor layer (0–10 km). Gehring et al. (2022) showed that orographic gravity waves induced strong alternating updrafts and downdrafts with a period of about 1 hour, clearly evident in W-band Doppler cloud radar velocity measurements. Radenz et al. (2021) inferred gravity-wave influence on cloud from lidar Doppler velocity time series using an autocorrelation-based approach, applying a threshold on the autocorrelation decay to distinguish coherent wave motions from turbulence. Kalesse and Kollias (2013) performed wavelet analysis on 10 second resolution time series of vertical air motion for 2 hour time windows and at each altitude to detect gravity waves. These studies demonstrate that high temporal and vertical resolution Doppler velocity measurements, such as those from the ship-based Marine W-band Cloud Radar (MWACR) during MARCUS, are well suited to detect high-frequency gravity waves and analyze their spectral characteristics within cloud environments.

Cyclones have previously been identified as sources of HFGWs, for example Nolan and Zhang (2017) showed from satellite imagery that tropical cyclones can efficiently generate short-wavelength HFGWs that radiate outward from the storm center, with tightly wrapped spiral wavefronts shaped by strong shear-induced differential advection and radial wavelengths of approximately 2–10 km. Southern Ocean cyclones are common throughout the year (Hoskins and Hodges, 2005; McErlich et al., 2023), with a maximum frequency in winter, and smaller-scale cyclones are common around the East Antarctic coast (Alexander and Murphy, 2015; Simmonds et al., 2012; Alexander et al., 2017; Irving et al., 2010), suggesting that cyclone-related forcing likely significantly contributes to HFGW activity in this region. However, this has not been systematically studied. In addition to cyclones, a statistical study of Antarctic gravity waves based on radiosonde data by Yoshiki and Sato (2000) suggested that some wave sources may reside in the stratosphere, with the polar night jet being a likely candidate. ERA5 reanalysis provides complete synoptic-scale wind fields (e.g., cyclones and jet streams), while MODIS satellite observations offer broad spatial coverage that captures the spatial structure of larger scale wave signatures (Vignon et al., 2020; Giongo et al., 2020; Gupta et al., 2021, 2024). Combining these datasets can help to track the large-scale background flow and identify potential wave sources.

Previous studies have greatly improved our understanding of GW activity over East Antarctica. The interaction between synoptic winds and coastal topography creates orographic gravity waves, and the temperature fluctuations caused by these waves

https://doi.org/10.5194/egusphere-2026-2155
Preprint. Discussion started: 30 April 2026

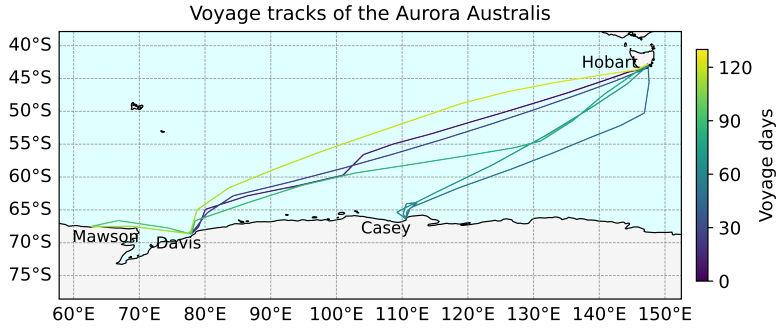

Figure 1. Voyage tracks of the Aurora Australis during the MARCUS field campaign, departing from Hobart, Australia, and proceeding to the Antarctic stations Davis, Casey, and Mawson. The colour bar indicates the number of voyage days.

affect the presence of local clouds (Alexander et al., 2017). One case study showed that a katabatic jumps can also lead to the trapping of gravity waves (Vignon et al., 2020). Cyclone-associated winds can also interact with coastal topography and katabatic flows, creating favorable conditions for the generation of orographic gravity waves along the East Antarctic coast (Orr et al., 2014). However, most existing studies have focused on individual case studies and on low-frequency gravity waves, while research on HFGWs, particularly those persisting over extended periods, remains scarce in this region.

The objective of this study is to identify and characterize long-lived high-frequency gravity wave activity observed using ship-based multi-platform observations over the Southern Ocean. We aim to distinguish HFGWs from other non-wave atmospheric oscillation processes, quantify their key wave properties and occurrence frequency over a broad spatial domain, investigate their possible sources and the background conditions that sustain multi-day wave activity. The potential influence of these waves on cloud properties is also identified.

This paper is organized as follows. Section 2 introduces the instruments and datasets. Section 3 describes the methodology for identifying HFGWs, as well as the ascent-rate analysis and FFT spectral techniques used to diagnose and characterize the observed wave signals. Section 4 presents the results. Section 4.1 demonstrates that the oscillations observed by the MWACR and radiosondes are gravity waves by ruling out alternative explanations, and quantifies their representative parameters and occurrence frequency. Section 4.2 investigates the possible sources of the observed HFGWs. Section 5 examines the background conditions that sustain the multi-day HFGW activity, the modulation of clouds by HFGWs, and proposes future research directions. Finally, Section 6 summarizes the main conclusions.

2 Instruments and datasets

During the MARCUS field campaign, a comprehensive suite of remote sensing and in-situ instruments from the U.S. Department of Energy (DOE) Atmospheric Radiation Measurement (ARM) Mobile Facility 2 (AMF2) operated onboard the Australian icebreaker *RSV Aurora Australis* (McFarquhar et al., 2021). These instruments provided observations of aerosols, clouds, precipitation, and radiation across the entire latitudinal range of the Southern Ocean between 29 October 2017 and

https://doi.org/10.5194/egusphere-2026-2155
Preprint. Discussion started: 30 April 2026

25 March 2018. Four voyages departed from Hobart (42.88°S, 147.32°E), Tasmania, including three to the Antarctic research stations Davis (68.58°S, 77.97°E), Casey (66.28°S, 110.53°E), and Mawson (67.60°S, 62.87°E), and one to Macquarie Island (54.50°S, 158.94°E), conducted in spring, summer, and autumn. Each round trip to Antarctica took 7–10 days, with stays at the research stations lasting up to two weeks (Mace et al., 2021). This study is based on data collected during the first three voyages (V1, V2, and V3) of the *RSV Aurora Australis*, with the corresponding ship tracks shown in Fig. 1. During V1, the vessel travelled from Hobart to Davis Station and remained there from 14 to 20 November 2017. During V2, the vessel first visited Casey Station, where it stayed from 21 December 2017 to 4 January 2018. It then undertook a second leg to Davis Station, remaining from 27 to 29 January 2018, followed immediately by a transit to Mawson Station, where it stayed from 1 to 17 February 2018. The vessel subsequently revisited Davis Station on 20 February 2018 for one day before returning to Hobart. The fourth voyage (V4) is not included in our analysis, as it was conducted along a different route toward Macquarie Island rather than the Antarctic region, and therefore falls outside the primary focus of this study. The ship's navigational location and attitude were logged every minute.

The MWACR provides vertical profiles of radar reflectivity (dBZ) and Doppler vertical velocity (i.e., the sum of particle fall speed and vertical air motion, m s^{-1}), with measurements acquired every 5 s and a vertical resolution of 30 m. The MWACR was mounted on a stabilized platform to maintain vertical pointing. Mace et al. (2021) compared subcloud liquid precipitation radar reflectivity from a calibrated BASTA cloud radar during CAPRICORN-II with that from the MARCUS MWACR over similar regions and during a common period, and found that applying a +4.5 dBZ offset to the MWACR reflectivity aligned the reflectivity distributions of the two radars. Consistent calibration offsets between the MWACR and the CloudSat cloud radar were also reported by Kollias et al. (2019), who showed that MWACR reflectivity was 4–8 dBZ lower. A uniform correction of +4.5 dBZ was therefore applied to all MWACR reflectivity observations used in this study. During the standard operating period along the east coast of Antarctica, the ship was located in calm nearshore waters where wave motion was strongly suppressed by sea ice (Vignon et al., 2021; Alexander et al., 2021). Consequently, ship heave, pitch, and roll were minimal, and the associated platform-motion-induced uncertainty in Doppler velocity was small and unlikely to affect the main conclusions of this study.

During MARCUS, radiosondes were launched four times daily, providing upper-air observations of dry bulb temperature, dew point temperature, and ascent rate up to approximately 25 km over the Southern Ocean and near the eastern Antarctic coastline, with a 2 s sampling interval. GPS measurements from the radiosondes were used to identify altitude and horizontal wind velocity components, namely the zonal (u) and meridional (v) winds, from which wind speed and direction were derived. Radiosonde data are used to examine fluctuations in the observed profiles and to assess whether they may be influenced by gravity waves or other processes, by calculating the Brunt–Väisälä frequency and the gradient Richardson number. A Total Sky Imager (TSI) also provides hemispheric images of cloud fields, which are used to identify wave-like cloud patterns potentially related to gravity waves (Black, 1983; Ugolnikov, 2023). A 532 nm micropulse lidar (MPL) provides backscatter and depolarization ratio data (Alexander and Protat, 2018). The data streams from the MPL and MWACR are combined into a merged lidar-radar cloud phase product, as described in Noh et al. (2019) and Alexander et al. (2021). Ice-phase clouds are identified from MPL measurements using linear functions of calibrated backscatter and layer depolarization (Hu et al., 2009), which are

https://doi.org/10.5194/egusphere-2026-2155
Preprint. Discussion started: 30 April 2026

integrated over the cloud to reduce inherent noise. Cloud temperatures below -40°C from ERA-Interim reanalysis were used as an additional constraint (Alexander and Protat, 2018).

ERA5, the fifth-generation reanalysis produced by the European Centre for Medium-Range Weather Forecasts (ECMWF), provides horizontal wind fields (u and v) at 700 and 250 hPa and vertical wind velocity at 800 hPa, representing near-surface and mid-to-upper tropospheric flow, together with geopotential fields. The data have a horizontal resolution of 0.25° × 0.25° and a temporal resolution of 1 hour (Hersbach et al., 2020) and numerous studies have shown their veracity in this region McErlich et al. (2023). The Aqua and Terra satellites each overpass the high latitudes of the Southern Hemisphere once during daylight, yielding cloud observations separated by approximately 4–6 hours. The Moderate Resolution Imaging Spectroradiometer (MODIS) instrument onboard the Aqua and Terra satellites provides corrected reflectance (MOD02HKM and MYD02HKM) at 500 m resolution for visualizing cloud fields and infrared brightness temperature (MOD021KM) at 1 km resolution for examining cloud-top temperatures. The MODIS Corrected Reflectance algorithm, developed by NASA/GSFC, removes major atmospheric effects (e.g., Rayleigh scattering) to produce true colour imagery (Gumley et al., 2003).

3 Methodology

Gravity wave events are primarily identified in this study using Doppler velocity measured by the ship-based MWACR. Doppler velocity measurements from the MWACR are used to detect coherent, periodic motions characteristic of gravity waves within clouds. TSI observations are used as a supplementary tool to provide independent visual confirmation of gravity-wave activity. Vertical displacements associated with gravity waves modulate cloud water content, leading to alternating bands, streaks, or periodic variations in cloud brightness that are directly observable in TSI images.

Perturbations in balloon ascent rates are used to characterize vertical motions during each sounding. The gradient Richardson number (Ri), derived from radiosonde temperature, pressure, and horizontal wind profiles, is used to assess the potential for turbulence. A small Richardson number ($0 < Ri < 0.25$) implies strong shear and active turbulence, whereas a large Richardson number ($Ri > 0.25$) indicates a stable atmosphere that is more likely to support gravity waves rather than turbulence.

Fast Fourier Transform (FFT) spectral analysis, combined with initial high-pass filtering, is applied to MWACR Doppler velocity data to identify oscillations related to gravity-wave frequencies. A high-pass filter is used to remove low-frequency variability, including linear trends, in time series used by the FFT. The original irregularly sampled measurements are interpolated onto uniform 60-s intervals. A Hamming window is applied to reduce spectral leakage, and the resulting amplitude attenuation is corrected using the coherent gain of the window. By padding the windowed time series with zeros to the nearest power-of-two length, the frequency sampling can be refined, allowing for clearer identification of dominant spectral peaks (Hocke and Wang, 2025). The resulting spectra are expressed in terms of calibrated Doppler vertical velocity amplitude, representing the relative strength of oscillations at each frequency in the Doppler velocity time series. To systematically identify gravity wave–induced oscillations, a sliding window analysis was applied using a temporal window of 2 hours and a vertical range of 2 km, similar to the procedure used in Kalesse and Kollias (2013). Within each window, the FFT was applied independently to the Doppler velocity time series at each height level within the 2-km layer. The resulting frequency spectra

https://doi.org/10.5194/egusphere-2026-2155
Preprint. Discussion started: 30 April 2026

were then averaged across heights to obtain a spectrum for that layer. We note that height levels influenced by liquid rain were excluded from the analysis. Oscillations were classified as gravity wave signals when the following criteria were satisfied: (1) the presence of a distinct dominant spectral peak with a period between 8 and 15 minutes was detected, and (2) a sufficiently pronounced peak amplitude, defined by a ratio of the main peak amplitude to secondary peaks greater than 1.3. The threshold value of 1.3 was empirically determined from the statistical characteristics of the full dataset, where secondary spectral peaks were consistently weaker than the dominant peak. This criterion ensures that only oscillations with a clearly defined dominant frequency are identified. Using these conditions, gravity wave-related oscillations were detected and their frequency of occurrence was subsequently estimated. For multi-layer clouds, cloud top and base heights were taken from the cloud layer corresponding to the height range of each HFGW-detected sliding window.

To assess whether the observed oscillations are consistent with gravity wave theory, several gravity-wave-related parameters are also examined. The frequency is estimated from FFT spectral analysis of the MWACR Doppler velocity time series and compared with the Brunt–Väisälä frequency N, derived from radiosonde potential temperature profiles when available. In addition, the vertical wavelength is estimated from the vertical phase gradient of the MWACR reflectivity. The probability density distribution is estimated using kernel density estimation (KDE), which provides a smoothed representation of the underlying data distribution.

4 Results

4.1 Evidence for High-Frequency Gravity Waves

Figure 2 shows examples of Doppler velocity and reflectivity measured by the MWACR near the Davis, Casey, and Mawson stations in East Antarctica during three different periods during the MARCUS campaign. The Doppler velocity is always negative, indicating the downward motion of hydrometeors, but exhibits alternating red and blue bands in each case with clear periodic variations linked to superimposed HFGWs. These oscillations exhibit strong vertical coherence, with minimal phase variation over the observed height range, indicating vertical wavelengths of several kilometres or longer. Typical examples are shown in Figs. 2(a) and (c), observed at Davis on 16–17 November 2017 and at Casey on 29–30 December 2017, respectively. In both cases, the Doppler velocity displays numerous bands with a characteristic period of approximately 10 minutes, within a cloud layer located between 4 and 8 km. Figure 3 shows that the cloud phase is predominantly ice in all three cases. At temperatures below –38 °C,the homogeneous freezing level, clouds are composed of ice. In Fig. 3 (a) and (b), sporadic occurrences of mixed-phase and supercooled liquid cloud are observed. The corresponding reflectivity fields (Fig. 2(b)) exhibit downward tilting reflectivity features, likely related to fall streaks. Figure 4 shows the cloud cover observed in a TSI image across the entire sky when the ship was near Davis station on 03:18 UTC on 17 November 2017. Striped cloud structures are evident in the TSI image, especially near the edge of the fisheye lens, and the clouds are relatively thin. ERA5 indicates that the horizontal wind is predominantly westerly and that wind shear is weak at the height of the cloud-layer in these cases. Figs. 2(e) and (f) show a case observed at Mawson on 8 February 2018, which exhibits similar features to the above, highlighting the ubiquitous nature of HFGWs. From 08:00 UT on 16 November to 08:00 UT on 18 November 2017, cloud conditions were favorable for

https://doi.org/10.5194/egusphere-2026-2155
Preprint. Discussion started: 30 April 2026

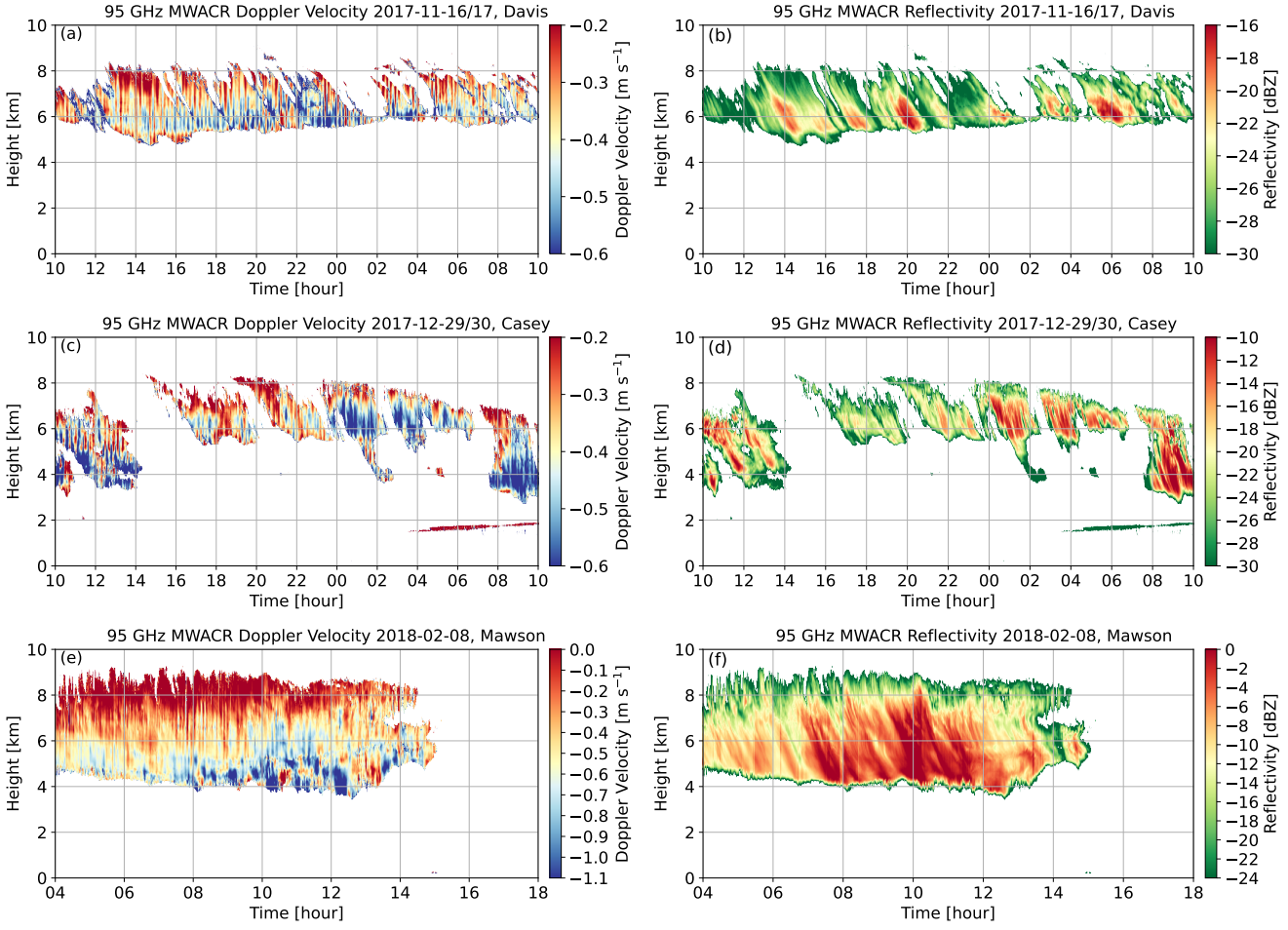

Figure 2. Doppler velocity (positive upward) and reflectivity observed by 95 GHz MWACR at Davis, Casey, and Mawson stations in East Antarctica. **(a, b)** Doppler velocity and reflectivity at Davis from 10:00 UTC on 16 November to 10:00 UTC on 17 November 2017. **(c, d)** Same as **(a, b)** but for Casey from 10:00 UTC on 29 December to 10:00 UTC on 30 December 2017. **(e, f)** Same as above but for Mawson from 05:00 UTC to 15:00 UTC on 8 February 2018.

FFT analysis, revealing a continuous 48-hour time interval for gravity wave monitoring (Figs. A1), representing an unusually long-lived HFGW event. The following section provides a detailed analysis of this event to investigate the gravity wave source and its characteristics. The range of radar reflectivity indicates that the size and concentration of cloud particles differ among the three cases. The low reflectivity values (e.g., -30 to -15 dBZ) suggest that the clouds are likely composed of small particles with low concentrations. Under such conditions, particle fall velocities are relatively small, allowing the Doppler velocity measured by the MWACR to more clearly represent vertical oscillations associated with atmospheric motions. Radiosonde data are unavailable for the Davis case (16–17 November 2017), and the vertical wavelength cannot be clearly identified from reflectivity in the Casey case (29–30 December 2017). Therefore, the analysis focuses on the Mawson case (8 February 2018).

https://doi.org/10.5194/egusphere-2026-2155
Preprint. Discussion started: 30 April 2026

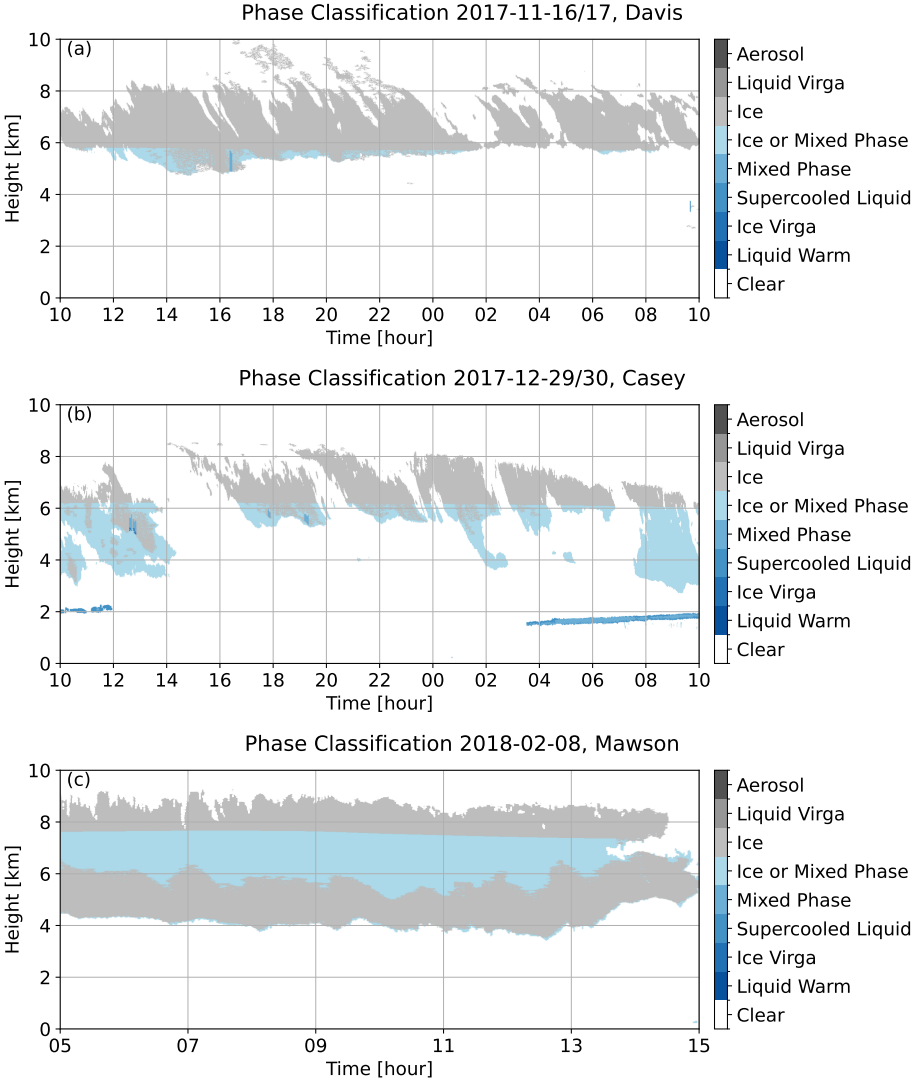

Figure 3. Cloud phase classification derived from MWACR and MPL at **(a)** Davis, **(b)** Casey, and **(c)** Mawson stations in East Antarctica. The time period corresponds to that shown in Fig. 2.

Figure 5 shows radiosonde profiles of dry-bulb temperature, potential temperature, dew point temperature, wind speed and direction, and ascent rate from three launches on 8 February 2018. The radiosondes launched at 05:30 and 11:30 UTC passed through or close to cloud layers, whereas the 17:30 UTC launch sampled cloud-free conditions after cloud dissipation at 15:00 UTC. Figs. 5(a) and (d) show weak, step-like temperature variations with amplitudes of approximately 0.3–0.7 °C within the
225 altitude range where the cloud layer is located. These intermittently distributed features correspond to statically stable layers in the troposphere, as evidenced by the potential temperature profiles. Regions where the dew point temperature is close to

https://doi.org/10.5194/egusphere-2026-2155
Preprint. Discussion started: 30 April 2026

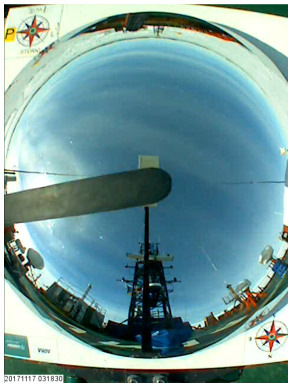

Figure 4. Total Sky Image (TSI) captured on 17 November 2027 at 03:18 UTC.

the dry-bulb temperature are associated with regions close to saturation and are associated with the presence of ice clouds in this case. For example, altitudes between 4 and 9 km in Figs. 5(a) and (d) show evidence of clouds. Figs. 5(b) shows that at 05:30 UTC, strong winds reaching up to 50 m s^{-1} are present at an altitude of around 9 km. At 11:30 and 17:30 UTC, Figs. 5(e) and (h), the wind speeds weakened markedly. Concurrently, wave-like structures developed, with the largest wave amplitude observed at 11:30 UTC in the ascent rate (see Figs. 5(f)). The wind direction shifts from east-southeasterly in the lower troposphere to west-northwesterly in the middle and upper troposphere in Figs. 5(b) and (e). As shown in Figs. 5(c), (f), and (i), the ascent rates of the three radiosondes launched at different times all exhibited significant fluctuations below 10 km altitude, these being particularly large at 11:30 UTC.

Fluctuations in the radiosonde ascent rate can arise from several processes, including convective generating cells, turbulence, and gravity waves. The formation of classical generating cells generally requires the presence of a liquid water layer, or at least substantial amounts of liquid water near the cloud top, to enable ice formation through ice-nucleation processes (Alexander et al., 2021). These conditions are unlikely in the ice clouds examined here, and the cloud-top cellular features observed after 12:00 UTC in Fig. 2(f) cannot be interpreted as generating cells. In addition, as shown in Fig. 6, the Richardson number is predominantly greater than 0.25, with only marginally lower values at a few levels, indicating conditions that are generally not favourable for the development of shear-induced turbulence. Overall, these results rule out convective generating cells and turbulence as the primary drivers of the observed ascent-rate fluctuations, favouring gravity waves as a more plausible explanation.

Figure 7 shows the Doppler velocity time series and the corresponding FFT spectra at 5.5 km altitude for 8 February 2018. The analysis period spans from 10:00 to 13:00 UTC, during which the Doppler velocity oscillations are particularly prominent, and whose midpoint (11:30 UTC) coincides with the radiosonde launch time. The FFT spectrum, shown in Fig. 7(b), exhibits a well-defined peak, with a dominant period of 10.24 minutes. The corresponding frequency, denoted by ω, is defined as $\omega = \frac{2\pi}{T}$ where T is the wave period. In this case, $\omega \approx 0.0102$ rad s^{-1}. This frequency is marginally smaller than the Brunt–Väisälä frequency $N = 0.0144$ rad s^{-1}, which corresponds to a period of 7.28 minutes. N is calculated from the radiosonde profile

https://doi.org/10.5194/egusphere-2026-2155
Preprint. Discussion started: 30 April 2026

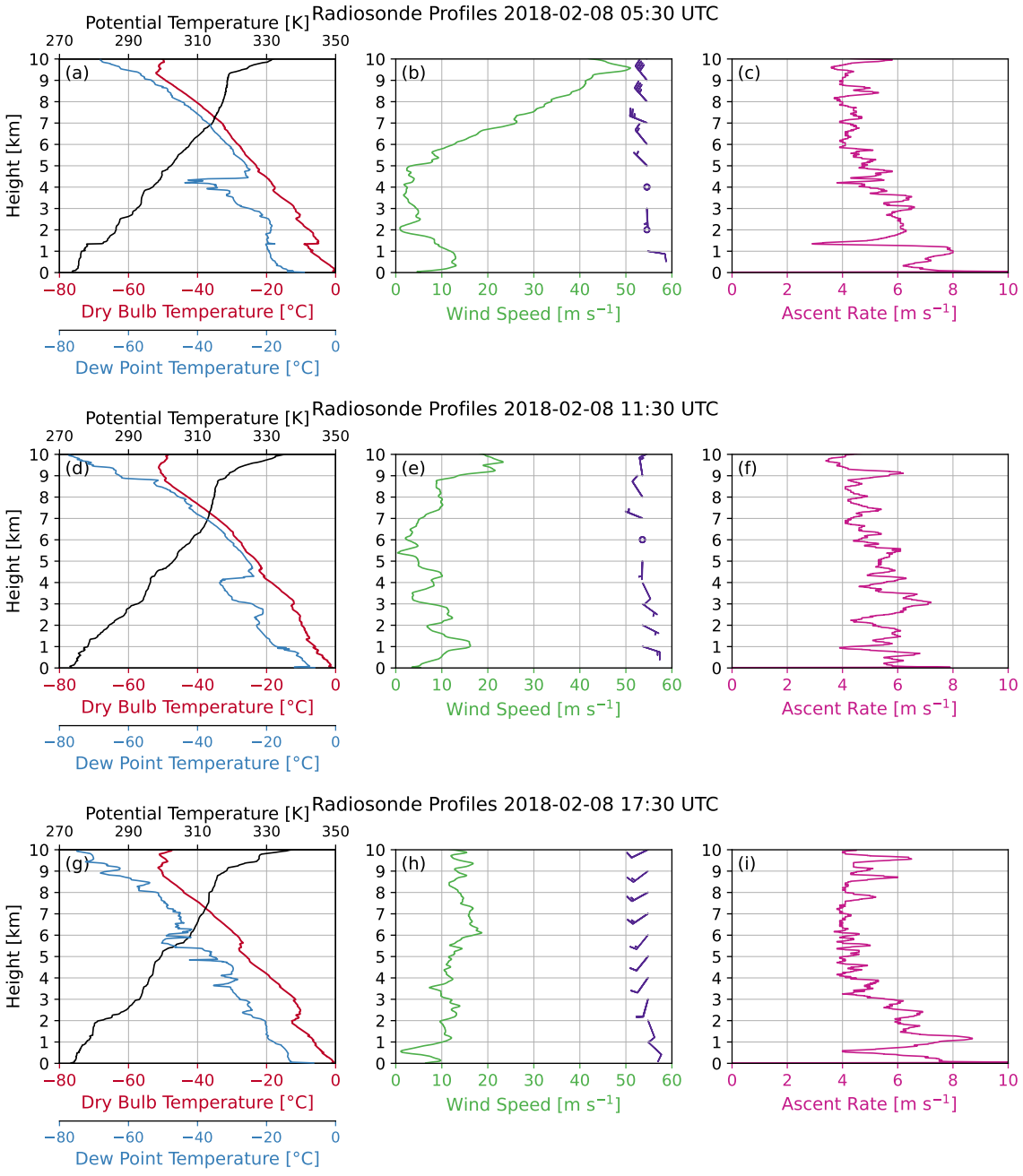

Figure 5. Dry bulb temperature, potential temperature, dew point temperature, wind speed, wind direction, and ascent rate profiles measured by radiosondes at Mawson, launched at **(a)–(c)** 05:30 UTC, **(d)–(f)** 11:30 UTC, and **(g)–(i)** 17:30 UTC on 8 February 2018.

https://doi.org/10.5194/egusphere-2026-2155
Preprint. Discussion started: 30 April 2026

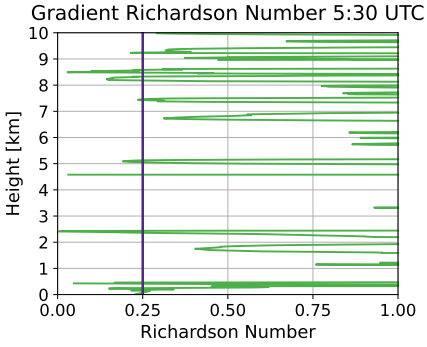

Figure 6. Richardson number (Ri) calculated from the corresponding radiosonde profile at 5:30 UTC on 8 February 2018. The vertical line at Ri = 0.25 denotes the Kelvin–Helmholtz instability threshold.

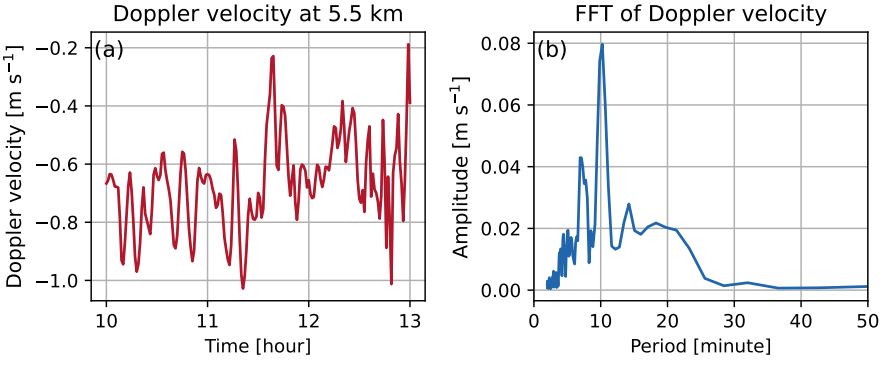

Figure 7. (a) Doppler velocity at 5.5 km observed by the MWACR at Mawson from 10:00 to 13:00 UTC on 8 February 2018. **(b)** Fast Fourier Transform (FFT) spectrum of the time series shown in **(a)**.

at an altitude centred on 5.5 km. These values satisfy the theoretical conditions for HFGWs, where the wave frequency ω lies between the inertial frequency f and the Brunt–Väisälä frequency N, and is close to N ($f < \omega \lesssim N$). The vertical spacing between successive reflectivity maxima (or banded structures) observed in the MWACR data suggests a vertical wavelength λ_z of approximately 3 km, which implies a horizontal wavelength of $\lambda_x = \lambda_z \sqrt{\frac{N^2}{\omega^2} - 1} \approx 2.97$ km. The corresponding vertical and horizontal wavenumbers are $m = 2.09 \times 10^{-3}$ rad m^{-1} and $k = 2.12 \times 10^{-3}$ rad m^{-1}, respectively. The horizontal phase speed of this wave can be estimated to be 4.83 m s^{-1}.

4.2 Potential Sources of the Observed Gravity Waves

The geographical settings differ among the three case studies considered (Fig. 2), yet all three locations exhibit HFGWs. At Davis, strong orographic gravity waves are typically observed under intense north-easterly flow associated with passing cy-

https://doi.org/10.5194/egusphere-2026-2155
Preprint. Discussion started: 30 April 2026

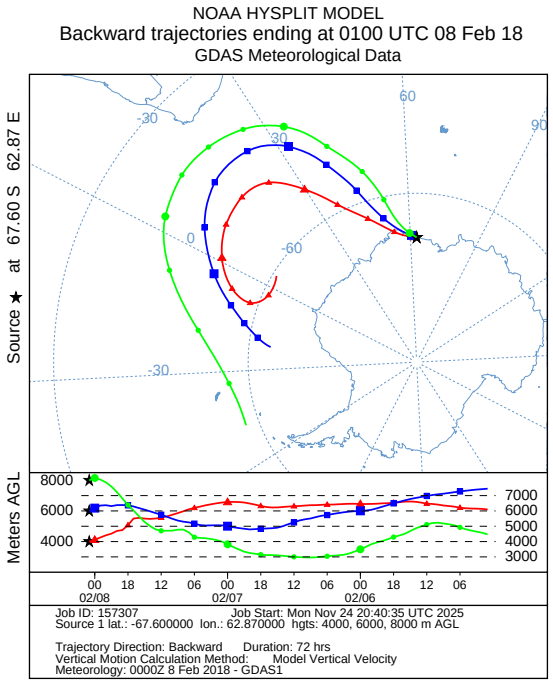

Figure 8. Back trajectory paths of the air mass that arrived at Mawson at 01:00 UTC on 8 February 2018. Trajectory calculations and visualization are provided by the NOAA HYSPLIT model and its online plotting system.

clones (Gehring et al., 2022). At Casey, strong wind events frequently arise from the combined influence of intense katabatic winds and enhanced synoptic-scale pressure-gradient forcing (Turner et al., 2001; Murphy and Simmonds, 1993). The wind regime at Mawson is more complex, dominated by south-easterly katabatic winds, although the station also experiences synoptic north-easterly flows during blizzard conditions or snowfall (Orr et al., 2014).

Lagrangian back trajectory analysis can be used to assess the origin of the observed air mass and whether it comes from low, middle or high latitudes where the amount of water vapor is different. Clouds can form locally, for example through the vertical ascent of water-vapour-rich air, or be transported by large-scale advection. Indicating whether an air mass passes over terrain or through a region of strong background flow helps to identify the potential source of gravity waves. Figure 8 shows back trajectories from the NOAA HYSPLIT model at three altitude levels (4, 6, and 8 km). The end time is set to 01:00 UTC, corresponding to the onset of cloud formation, and the star marks the location of Mawson. As shown in Fig. 8, the cloud-associated air mass is entirely of oceanic origin. Cyclonic activity initially transports these air masses northward or north-eastward across the open ocean, after which they are advected south-eastward by subsequent cyclonic activity and the prevailing large-scale flow, eventually reaching the coastline near Mawson. In addition to modulating air mass transport, cyclones are also recognized as an important source of HFGWs (e.g., Nolan and Zhang, 2017). Air parcels originating at lower levels experience long-range transport before ascending to higher altitudes.

Figure 9 shows the ERA5 horizontal wind field at 700 hPa superimposed over the topography, the vertical velocity at 800 hPa,

https://doi.org/10.5194/egusphere-2026-2155
Preprint. Discussion started: 30 April 2026

and the horizontal wind fields at 250 hPa. The 700 and 800 hPa winds show the lower-tropospheric flow and are analysed to assess whether topographic forcing could contribute to gravity-wave generation, while the 250 hPa winds represent the upper-tropospheric circulation and are analysed to diagnose the likelihood of jet-related gravity-wave sources in this case, motivated by the strong winds observed by the radiosonde at 05:30 UTC. Figure 9(a) shows that the low-level wind field is characterized by both katabatic flow and a cyclone. The positive pressure vertical velocity near the Mawson site in Fig. 9(b) also indicates large-scale subsidence. Such katabatic winds interacting with the steep coastal slopes of the Antarctic ice sheet can generate orographic gravity waves (Grazioli et al., 2017; Watanabe et al., 2006). The spiralling cyclonic winds near Mawson Station are predominantly east-southeasterly, consistent with the wind direction shown in Fig. 5(b), with wind speeds gradually increasing toward the centre of the low pressure system. Figure 10 displays a MODIS/Aqua satellite image of the associated clockwise-rotating cyclone, which extends over roughly 20° of longitude and represents a large-scale (synoptic) system with embedded small-scale clouds in the region behind the cold front. Figure 9(c) illustrates the meandering trajectory of the polar jet, with wind speeds in the jet core reaching up to 76 m s^{-1}, resulting in a west-northwest flow near Mawson. Overall, strong and stable stratification, polar jet streams and coastal katabatic winds, together with frequent cyclone activity (Hoskins and Hodges, 2005), create a favorable large-scale environment for the widespread occurrence of HFGWs near the East Antarctic coastline.

These HFGWs are also observed at numerous locations over the Southern Ocean, far from the coast, during MARCUS (Fig. 1). In these regions, topographic forcing cannot be the primary driver. Instead, the waves are probably generated by synoptic-scale systems such as cyclones and fronts which are frequently observed in this region.

4.3 Statistical analysis of MARCUS HFGWs

The ship's stabilized platform malfunctioned on 2 December 2017 and could no longer provide a stable mounting for the MWACR. This reduced the quality of the Doppler velocity measurements and prevented the reliable identification of vertical oscillations. Figure 11(a) and (d) illustrates time series of HFGW amplitude and period derived from FFT analysis. Shaded areas in the figure indicate periods excluded due to missing or flagged data in the ARM repository. After removing these intervals, a total of 57 days of valid observations remain. These include periods when the vessel was stationary near the coastline, as well as the initial phase of stabilized platform operation. Figure 2 further demonstrates that MWACR measurements obtained during these stationary coastal periods remain reliable. During these 57 days, clouds are observed for a total of 62,859 minutes, among which 28,680 minutes exhibited periodic oscillations in the MWACR Doppler velocity, accounting for 46% of the time that waves could have been observed. These oscillations occurred on 52 out of 57 days, accounting for 91% of all the days where reliable data was available. These 52 days are mainly concentrated before 2 December 2017 and during periods when the research vessel exhibited minimal horizontal movement near the three Antarctic research stations, as shown in Fig. 1.

As shown in Fig. 11(a), the detected vertical velocity amplitudes are mostly around 0.02 m s^{-1}. The KDE-based density distribution in Fig. 11(b) suggests a slightly higher occurrence of oscillations at Davis. At Mawson, a pronounced enhancement is evident during 1–6 February 2018 in Fig. 11(a). By comparison, Casey exhibits a lower occurrence frequency than the other

https://doi.org/10.5194/egusphere-2026-2155
Preprint. Discussion started: 30 April 2026

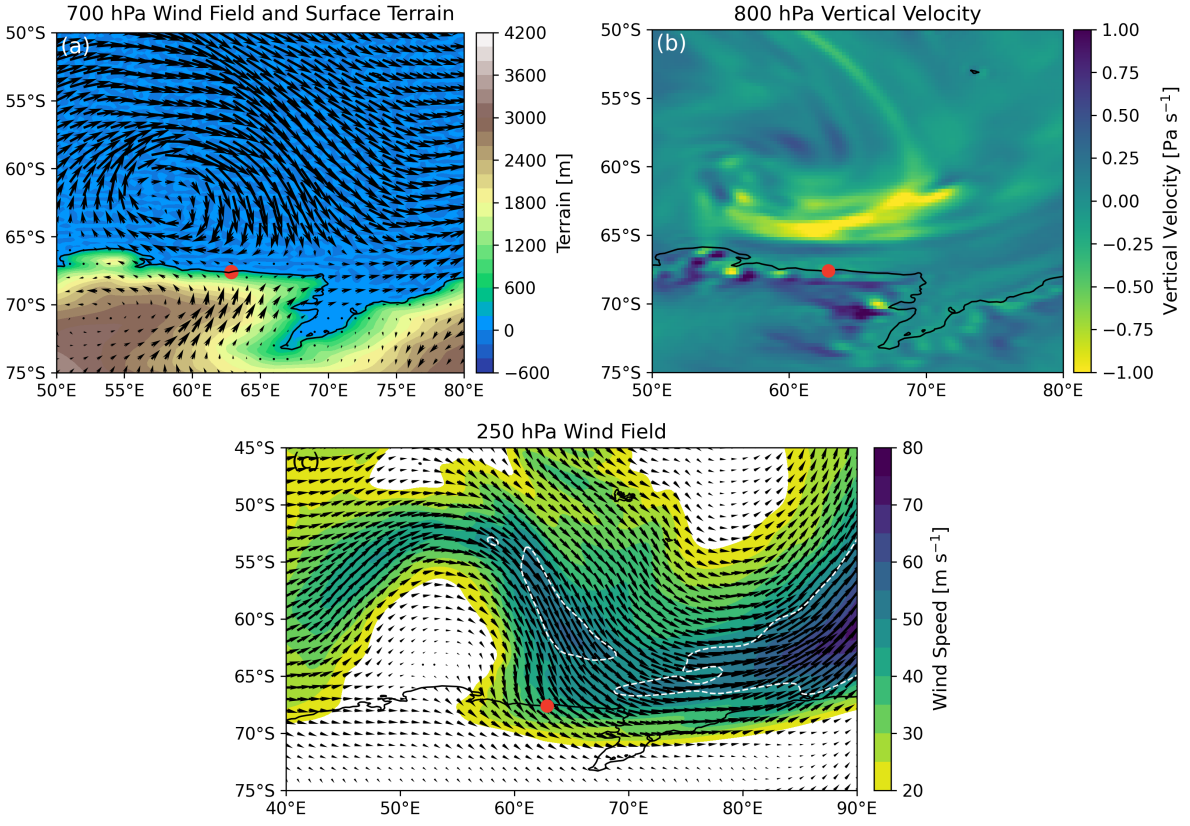

Figure 9. (a) Horizontal wind field at 700 hPa and surface terrain from the ERA5 reanalysis over Mawson at 05:30 UTC on 8 February 2018. **(b)** Vertical velocity at 800 hPa. **(c)** Horizontal wind field at 250 hPa. Arrows represent horizontal wind vectors, with direction indicating the airflow and length proportional to wind speed. The red dot marks Mawson station. The white dashed contour indicates regions where wind speeds exceed 50 m s^{-1}.

two sites. Figure 11(c) presents the temporal classification of cloud conditions, including cloud-free periods, clouds without HFGWs, and clouds with HFGWs. Examination of Fig. 11(c) reinforces the ubiquitous nature of these waves and the frequent occurrence of extended continuous periods of wave activity, greater than 2 hours and up to 48 hours, at all three sites. Highlighting that these waves are very common when observations are available to identify them. Binning the detected HFGW periods in Fig. 11(d) indicates that the majority of waves occur between 9–12 minutes, with a peak frequency in the 10–11 minute bin. The corresponding angular frequencies ω are approximately 0.009–0.012 rad s^{-1}. These characteristics are consistent with small-amplitude gravity waves. No significant variation in amplitude with period is observed. The amplitudes in the vertical Doppler velocity remain concentrated around 0.02 m s^{-1} across all periods, which is consistent with the high-density regions in the KDE plot in Fig. 11 (a). Figure 11 (e) displays the latitude of the vessel as a function of time. Comparison of the HFGW amplitudes with the latitude of the vessel shows little sign of a latitudinal variation. This implies that the different sources

https://doi.org/10.5194/egusphere-2026-2155
Preprint. Discussion started: 30 April 2026

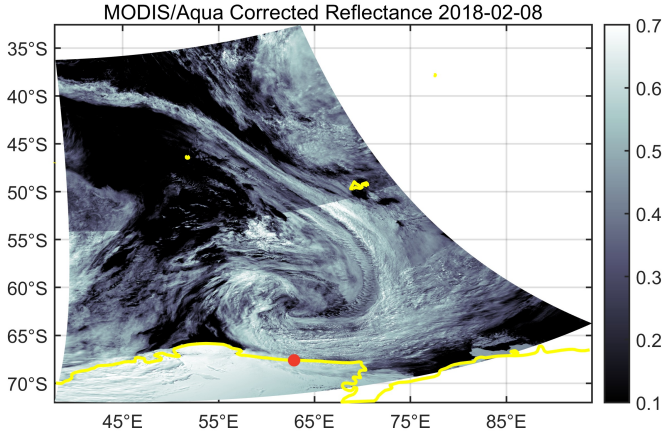

Figure 10. Corrected reflectance from MODIS/Aqua over Mawson on 8 February 2018. The yellow line indicates the coastline, and the red dot marks the Mawson station.

detailed in Section 4.2 produce gravity waves of comparable magnitudes since the katabatic forcing would only be observed near the East Antarctic coastline. Potentially highlighting that frontal and jet sources dominate.

Figure 12 presents the cloud base, cloud top, and cloud thickness for all clouds sampled by the MWACR and for clouds influenced by HFGWs. The comparison highlights the effect of HFGWs relative to the overall cloud population. For all clouds, the cloud base peaks near the lowest observable altitude of the MWACR (approximately 230 m above sea level), reflecting the dominance of shallow boundary-layer clouds over the Southern Ocean (Tansey et al., 2023). In contrast, clouds with HFGWs exhibit an additional peak in cloud base height at around 4 km. Cloud tops for all clouds are mostly around 2 km, whereas clouds with HFGW peak at 8 km. Similarly, cloud thickness is 1 km for all clouds and 2.5 km for clouds where HFGW were observed. These clouds are typically distributed between the 0 °C isotherm and the homogeneous freezing threshold, suggesting the presence of mixed-phase and supercooled liquid water. The elevated cloud tops (8 km) of clouds where HFGW were present possibly suggests a possible connection to polar jet stream dynamics. Effectively an enhanced occurrence of HFGW presence for clouds with higher cloud tops may signal a jet related source is important.

5 Discussion

The three events share several common features beyond the periodic Doppler velocity oscillations. First, the clouds in all three cases are mainly ice or mixed phase, with cloud tops peaking near 8 km altitude. Second, during these events, the dominant oscillation periods are consistently within the range of 10–15 minutes. For Davis and Casey, FFT spectral analysis of the Doppler velocity during periods of pronounced oscillations yields dominant periods of 13.3 minutes and 11.6 minutes, respectively. Third, the air masses associated with these three events all originated from the north-west and were transported over long distances toward the East Antarctic coast. Fourth, large-scale cyclones were present in the vicinity of the observation sites during all three events (Figs. B1 and B2).

https://doi.org/10.5194/egusphere-2026-2155
Preprint. Discussion started: 30 April 2026

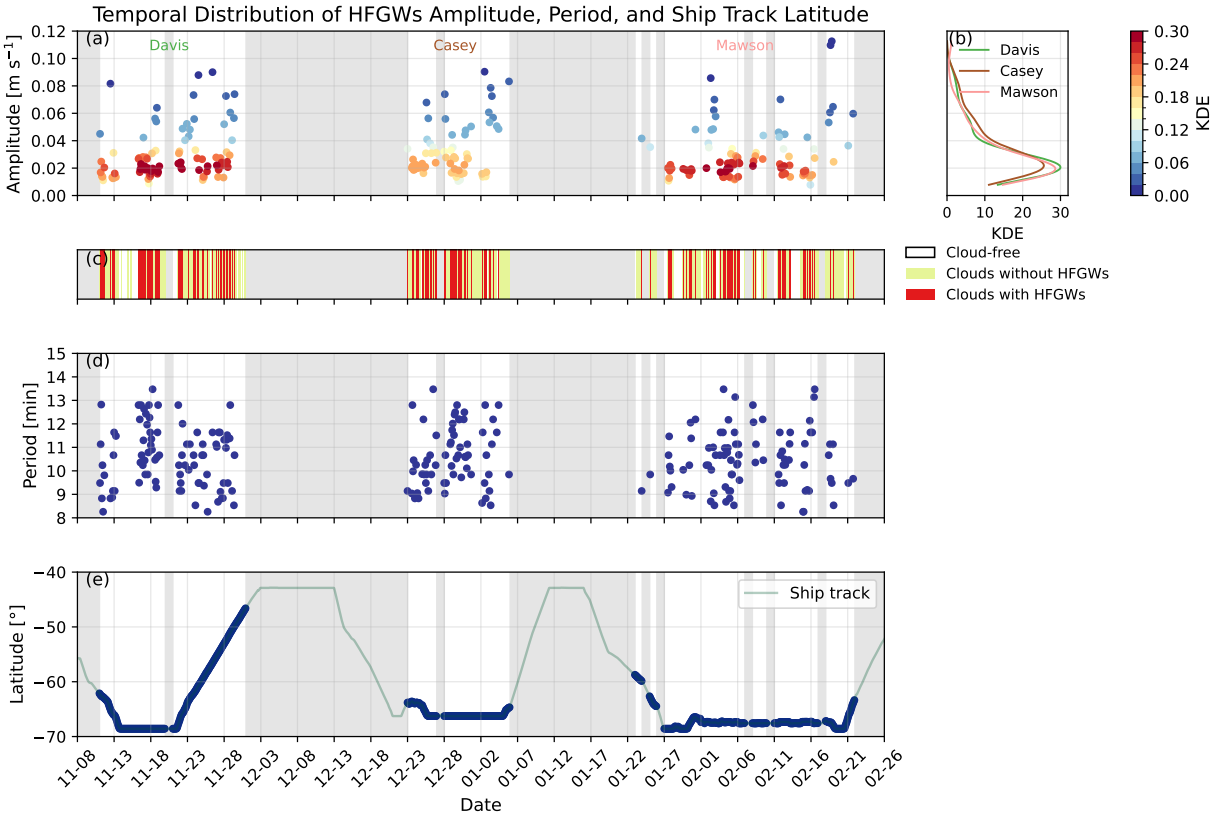

Figure 11. **(a)** Scatter plot of detected gravity wave amplitudes over time. Each point shows the dominant spectral peak within a 2-hour × 2-km sliding window, with color indicating local point density estimated via kernel density estimation (KDE). **(b)** KDE of gravity wave amplitudes for the three selected periods corresponding to Davis, Casey, and Mawson stations. **(c)** Temporal distribution of cloud-free conditions, clouds without HFGWs, and clouds with HFGWs. **(d)** Scatter plot of detected gravity wave periods over time, with points corresponding to the same sliding windows as in **(a)**. **(e)** Latitude of the ship track at the times of detected high-frequency gravity wave signals. Each point highlighting the time of the detected peaks along the ship track.

In addition to HFGWs, cloud observations from MWACR and MPL exhibit pronounced low-frequency variability occasionally. As shown in Fig. 13, the MWACR cloud mask (Fig. 13(a)) and MPL backscatter (Fig. 13(b)) from 16:00 to 00:00 UTC display a wave-like variation in cloud-base height, likely associated with periodic lifting and lowering of the cloud layer induced by vertical displacements related to gravity waves. The characteristic period of this variability is approximately 2 hours and is likely associated with lower-frequency gravity waves superimposed on a slowly varying background, producing quasi-periodic oscillations on multi-hour timescales. The coexistence of low-frequency vertical velocity variability and HFGWs indicates a multiscale dynamical environment, where the low-frequency background might maintain stable stratification and quasi-steady conditions, favoring repeated excitation of HFGWs and their persistence over tens of hours.

To assess whether the observed HFGWs in this case are supported by ducting conditions, the vertical structure of temperature

https://doi.org/10.5194/egusphere-2026-2155
Preprint. Discussion started: 30 April 2026

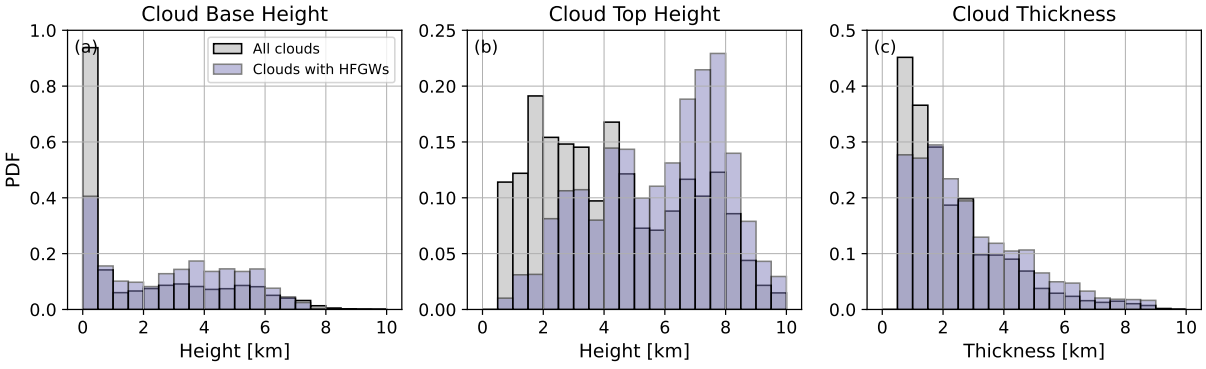

Figure 12. Probability density functions (PDFs) derived from normalized histograms. **(a)** Cloud base height and **(b)** cloud top height for all clouds in the sample and for clouds with HFGWs, identified based on periodic oscillations in MWACR Doppler velocity. **(c)** Cloud thickness, defined as the difference between cloud top and base heights.

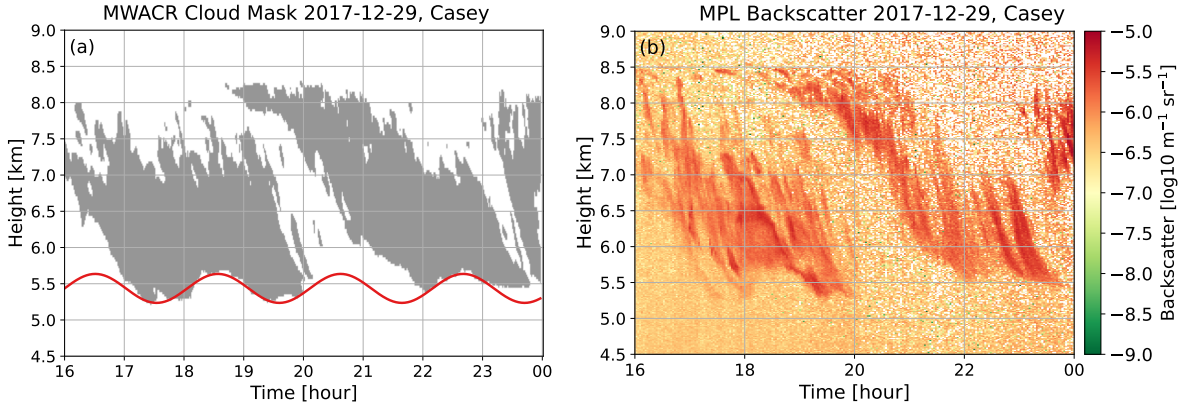

Figure 13. (a) Cloud mask observed by MWACR at Casey from 16:00 to 00:00 UTC on 29 December 2017. The red solid line represents smoothed sinusoidal curve of cloud base height. **(b)** Backscatter observed by MPL.

and static stability is analysed using radiosonde observations. The step-like radiosonde temperature structure in Figs. 5(a), (d), and (g) indicates inversions in the troposphere. The corresponding squared Brunt–Väisälä (buoyancy) frequency, $N^2 = \frac{g}{\theta}\frac{\partial\theta}{\partial z}$, is shown in Fig. 14, where g is the gravitational acceleration, θ is the potential temperature, and z is altitude. Within the 05:30 UTC inversion layer (Fig. 14 (a)), radiosonde data at 1.5 km indicates a maximum N^2 exceeding 12×10^{-4} s^{-2}, representing a strongly stratified layer near the surface. Between approximately 8 km and 9 km, N^2 approaches zero, indicating very weak stratification, while above 9 km the value increases sharply. Such a vertical structure is conducive to the formation of thermal ducts, which can trap gravity waves and suppress vertical energy propagation (Fritts and Alexander, 2003). The calculated local buoyancy period is typically 5–10 minutes. Given the relatively weak background winds (mean speed < 10 m s^{-1} below 8 km), Doppler shifting is likely negligible in this case. The strong near-surface inversion combined with weak stratification

https://doi.org/10.5194/egusphere-2026-2155
Preprint. Discussion started: 30 April 2026

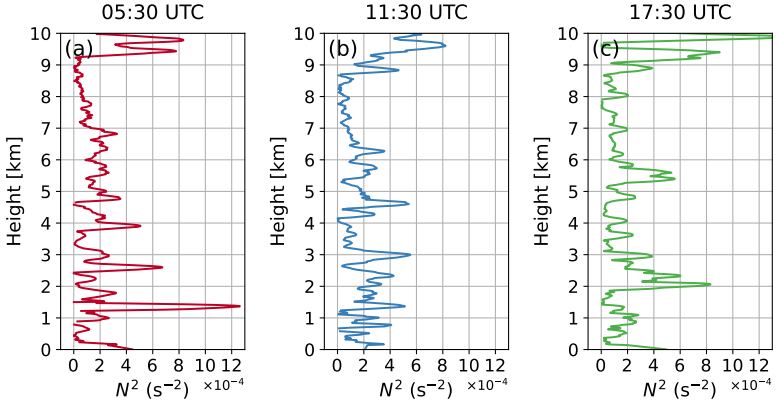

Figure 14. Squared Brunt–Väisälä (buoyancy) frequency profiles derived by radiosonde at Mawson on 8 February 2018 at **(a)** 05:30 UTC, **(b)** 11:30 UTC, and **(c)** 17:30 UTC.

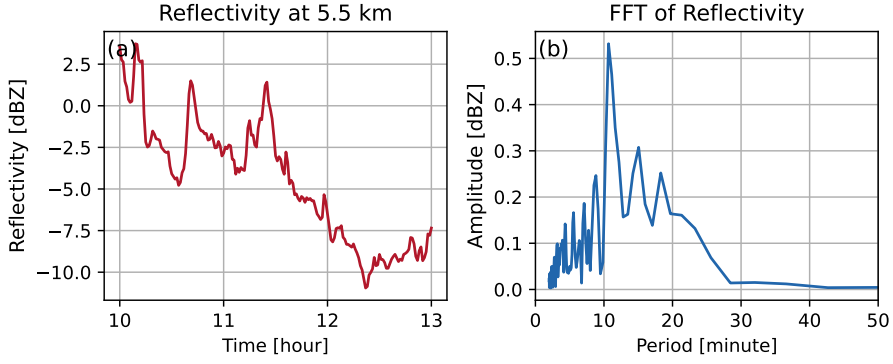

Figure 15. **(a)** Reflectivity at 5.5 km observed by MWACR at Mawson from 10:00 to 13:00 UTC on 8 February 2018. **(b)** Fast Fourier Transform (FFT) spectrum of the time series shown in **(a)**.

aloft effectively traps HFGWs. The persistence of the observed waves further suggests limited turbulent dissipation, allowing HFGWs to remain confined below 8 km for more than 48 h.

In addition to the low frequency variability in cloud base, variations in other cloud properties are also observed. For example, MWACR reflectivity is analysed to assess whether HFGWs influence cloud properties. HFGWs are not expected to occur only under cloudy conditions; however, the presence of clouds provides scattering targets that allow the MWACR to detect associated dynamical disturbances. As shown in Fig. 15, the MWACR reflectivity exhibits a clear periodic signal in the FFT spectrum, with a dominant period of 10.67 minutes, which is close to the 10.24-minute period derived from Doppler velocity. This suggests that HFGWs also modulate cloud properties such as particle concentration or growth processes within the cloud layer.

Future research will focus on the role of HFGWs in modulating Antarctic cloud and precipitation properties. In tropical regions,

https://doi.org/10.5194/egusphere-2026-2155
Preprint. Discussion started: 30 April 2026

HFGW-induced temperature perturbations have been shown to enhance ice nucleation by increasing cooling rates, thereby increasing ice crystal concentrations in clouds (Jensen et al., 2016; Schoeberl et al., 2016). However, to our knowledge, no comparable studies have been conducted in Antarctica. Extending this analysis to East Antarctica would help determine whether similar HFGW–cloud microphysical mechanisms operate under polar conditions and assess their impacts on cloud lifetime, precipitation, and the surface energy balance. Such work will require multi-instrument observations, including measurements of cloud condensation nuclei (CCN) and Ice Nucleating Particles (INP). Another promising direction is to investigate the impact of HFGWs on virga. For example, we could use the Virga-sniffer tool detailed in Kalesse-Los et al. (2023) to check if virga is observed more frequently during periods when HFGWs are present. Virga (snow and ice virga) is a common precipitation feature in Antarctica, in which falling ice particles or snow sublimate in the lower atmosphere and can indirectly influence the Antarctic ice mass balance (Grazioli et al., 2017). Building on our results, future studies could examine how HFGW-induced vertical motion and turbulence modulate virga formation, sublimation rates, and precipitation efficiency, potentially linking gravity wave activity to the broader Antarctic cloud–precipitation system.

6 Conclusions

Using 57 days of valid Doppler vertical velocity measurements from a ship-based cloud radar during the MARCUS campaign (November 2017–February 2018), analysis indicates that HFGWs are detected approximately 46% of the time that cloud is observed and on about 91% of cloudy days, with waves persisting continuously for up to 48 hour under favorable conditions. These waves typically have amplitudes of around 0.02 m s^{-1} and are often found in clouds with tops near 8 km.

Similar periodic Doppler velocity oscillations are observed at different times at three Antarctic coastal sites (Davis, Casey, and Mawson), with the affected clouds predominantly consisting of ice or mixed-phase particles. A detailed case study at Mawson on 8 February 2018 reveals weak step-like temperature structures indicative of stable layers, accompanied by pronounced fluctuations in radiosonde ascent rates. Ice clouds likely exclude the formation of convective generating cells, and gradient Richardson numbers rarely fell below 0.25 in this case, suggesting that turbulence is unlikely. FFT spectral analysis and parameter estimation further confirm that the observed oscillations satisfy the theoretical criteria for HFGWs, exhibiting periods of about 10 minutes and horizontal wavelengths of approximately 3 km. Observed reflectivity variations at Mawson further indicate that HFGWs can modulate cloud properties.

Air-mass trajectories indicate that for the MAwson case study the flow originated from the northwest and underwent long-range transport. Combined analysis of ERA5 reanalysis and MODIS satellite observations suggests that HFGWs over East Antarctica in this case are likely generated by the combined effects of the polar jet stream, coastal katabatic winds, and frequent cyclonic activity. Furthermore, MWACR and MPL measurements indicate the presence of low-frequency gravity wave activity and thermal ducts, which can sustain HFGWs for tens of hours. This study provides observational evidence that HFGWs are a common and persistent component of Antarctic atmospheric dynamics, highlighting their potential influence on clouds and local-scale processes, which could inform improvements in atmospheric modeling.

https://doi.org/10.5194/egusphere-2026-2155
Preprint. Discussion started: 30 April 2026

Appendix A: 48-hour continuous gravity wave

Figs. A1 show the MWACR Doppler velocity at Davis from 08:00 UTC on 16 November to 08:00 UTC on 18 November 2017. During this 48-hour period, FFT analysis failed to detect oscillations in Doppler velocity only between 10:00 and 12:00 UTC on 17 November, due to the absence of clouds.

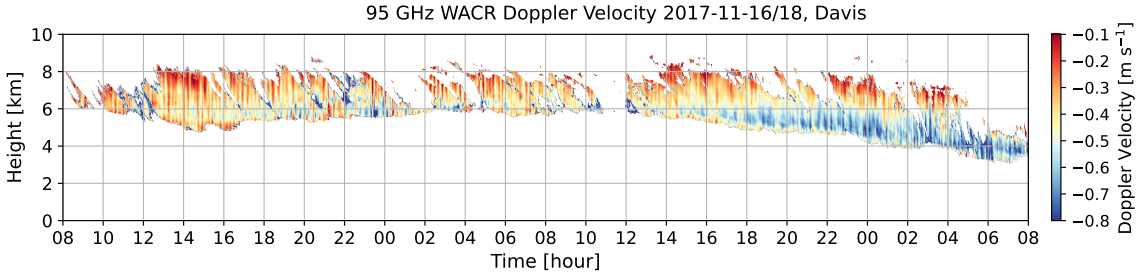

Figure A1. Doppler velocity at Davis from 08:00 UTC on 16 November to 08:00 UTC on 18 November 2017.

Appendix B: MODIS observations of cloud conditions over Davis and Casey

Figs. B1 and B2 show MODIS corrected reflectance over Davis on 17 November 2017 and over Casey on 29 December 2017, respectively. The infrared brightness temperature in Fig. B1(b) reveals distinct striped cloud bands near Davis and located along the edge of a cyclone, indicating that these clouds were modulated by gravity waves.

https://doi.org/10.5194/egusphere-2026-2155
Preprint. Discussion started: 30 April 2026

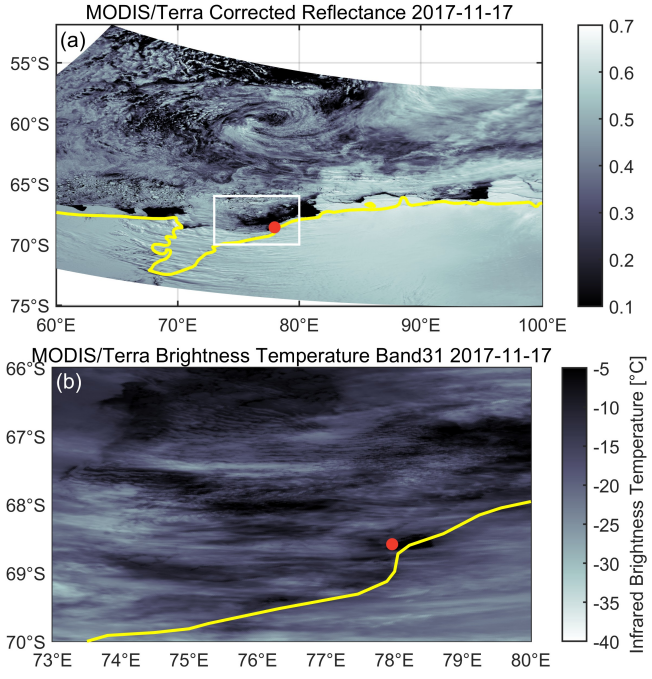

Figure B1. (a) Corrected reflectance from MODIS/Terra over Davis on 17 November 2017. The yellow line indicates the coastline, and the red dot marks the Davis station. **(b)** Zoomed-in view of the white box in **(a)** shown with infrared brightness temperature.

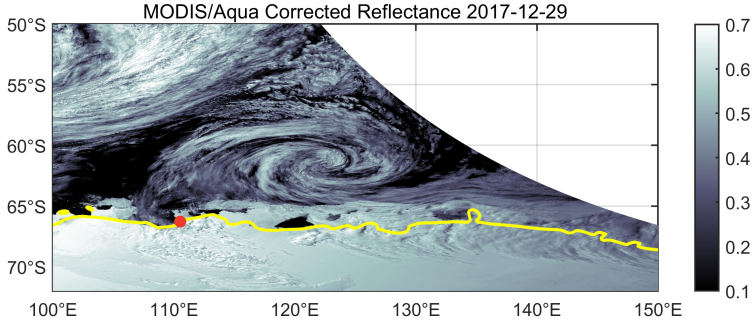

Figure B2. Corrected reflectance from MODIS/Aqua over Casey on 29 December 2017. The yellow line indicates the coastline, and the red dot marks the Casey station.

Data availability. MARCUS data were obtained from the Atmospheric Radiation Measurement (ARM) Program, sponsored by the U.S. Department of Energy, Office of Science, Office of Biological and Environmental Research, and Climate and Environmental Sciences Division. We thank the ARM technicians for collecting the data and maintaining the instruments onboard RSV *Aurora Australis*. ARM-

https://doi.org/10.5194/egusphere-2026-2155
Preprint. Discussion started: 30 April 2026

MARCUS data used in this study are available from the ARM Data Center (https://adc.arm.gov/discovery/). ERA5 data can be accessed via the Copernicus Climate Data Store (https://cds.climate.copernicus.eu/). MODIS satellite imagery is available through NASA Worldview (https://worldview.earthdata.nasa.gov/). Ship surface meteorological and position data are provided by the Australian Antarctic Data Centre (https://data.aad.gov.au). All datasets are freely available upon registration.

Author contributions. WW, AM, and KH designed the study concept, with input from SA. WW developed the methodology with contributions from AM, SA, and KH. SA was responsible for cloud phase classification and lidar processing. WW performed the data analysis and drafted the manuscript. All authors contributed to the interpretation of the results and reviewed the manuscript.

Competing interests. The authors declare that they have no conflict of interest.

Disclaimer. Publisher's note: Copernicus Publications remains neutral with regard to jurisdictional claims in published maps and institutional affiliations.

Acknowledgements. Wenyue Wang gratefully acknowledges financial support from the Swiss National Science Foundation (SNSF; grant no. 225384). The lead author also thanks Prof. Dr. Heike Kalesse-Los and Dr. Alex Schuddeboom for helpful discussions. Technical, logistical, and ship support for MARCUS were provided by the Australian Antarctic Division through Australian Antarctic Science Projects 4292 and 4387, and we thank Steven Whiteside, Lloyd Symonds, Rick van den Enden, Peter de Vries, Chris Young, and Chris Richards for their assistance. Adrian McDonald acknowledges the funding from the Ministry of Business, Innovation and Employment Smart Idea scheme (UOC2501).

https://doi.org/10.5194/egusphere-2026-2155
Preprint. Discussion started: 30 April 2026

References

Alexander, M. J., Holton, J. R., and Durran, D. R.: The Gravity Wave Response above Deep Convection in a Squall Line Simulation, Journal of Atmospheric Sciences, 52, 2212 – 2226, https://doi.org/10.1175/1520-0469(1995)052<2212:TGWRAD>2.0.CO;2, 1995.

Alexander, M. J., Beres, J. H., and Pfister, L.: Tropical stratospheric gravity wave activity and relationships to clouds, Journal of Geophysical Research: Atmospheres, 105, 22 299–22 309, https://doi.org/10.1029/2000JD900326, 2000.

Alexander, S. and Murphy, D.: The Seasonal Cycle of Lower-Tropospheric Gravity Wave Activity at Davis, Antarctica (69°S, 78°E), Journal of the Atmospheric Sciences, 72, 1010 – 1021, https://doi.org/10.1175/JAS-D-14-0171.1, 2015.

Alexander, S. P. and Protat, A.: Cloud Properties Observed From the Surface and by Satellite at the Northern Edge of the Southern Ocean, Journal of Geophysical Research: Atmospheres, 123, 443–456, https://doi.org/10.1002/2017JD026552, 2018.

Alexander, S. P., Klekociuk, A. R., Pitts, M. C., McDonald, A. J., and Arevalo-Torres, A.: The effect of orographic gravity waves on Antarctic polar stratospheric cloud occurrence and composition, Journal of Geophysical Research: Atmospheres, 116, https://doi.org/10.1029/2010JD015184, 2011.

Alexander, S. P., Sato, K., Watanabe, S., Kawatani, Y., and Murphy, D. J.: Southern Hemisphere Extratropical Gravity Wave Sources and Intermittency Revealed by a Middle-Atmosphere General Circulation Model, Journal of the Atmospheric Sciences, 73, 1335 – 1349, https://doi.org/10.1175/JAS-D-15-0149.1, 2016.

Alexander, S. P., Orr, A., Webster, S., and Murphy, D. J.: Observations and fine-scale model simulations of gravity waves over Davis, East Antarctica (69°S, 78°E), Journal of Geophysical Research: Atmospheres, 122, 7355–7370, https://doi.org/10.1002/2017JD026615, 2017.

Alexander, S. P., McFarquhar, G. M., Marchand, R., Protat, A., Vignon, É., Mace, G. G., and Klekociuk, A. R.: Mixed-Phase Clouds and Precipitation in Southern Ocean Cyclones and Cloud Systems Observed Poleward of 64°S by Ship-Based Cloud Radar and Lidar, Journal of Geophysical Research: Atmospheres, 126, e2020JD033 626, https://doi.org/10.1029/2020JD033626, 2021.

Baumgaertner, A. J. G. and McDonald, A. J.: A gravity wave climatology for Antarctica compiled from Challenging Minisatellite Payload/Global Positioning System (CHAMP/GPS) radio occultations, Journal of Geophysical Research: Atmospheres, 112, https://doi.org/10.1029/2006JD007504, 2007.

Black, P.: Tropical storm structure revealed by stereoscopic photographs from Skylab, Advances in Space Research, 2, 115–124, 1983.

Cao, B. and Liu, A. Z.: Statistical Characteristics of High-Frequency Gravity Waves Observed by an Airglow Imager at Andes Lidar Observatory, Earth and Space Science, 9, e2022EA002 256, https://doi.org/10.1029/2022EA002256, 2022.

Chang, S., He, H., and Huang, D.: The effects of gravity waves on ozone over the Tibetan Plateau, Atmospheric Research, 299, 107 204, https://doi.org/10.1016/j.atmosres.2023.107204, 2024.

Franco-Diaz, E., Gerding, M., Holt, L., Strelnikova, I., Wing, R., Baumgarten, G., and Lübken, F.-J.: Convective gravity wave events during summer near 54° N, present in both AIRS and Rayleigh–Mie–Raman (RMR) lidar observations, Atmospheric Chemistry and Physics, 24, 1543–1558, https://doi.org/10.5194/acp-24-1543-2024, 2024.

Fritts, D. C. and Alexander, M. J.: Gravity wave dynamics and effects in the middle atmosphere, Reviews of Geophysics, 41, https://doi.org/https://doi.org/10.1029/2001RG000106, 2003.

Gehring, J., Vignon, É., Billault-Roux, A.-C., Ferrone, A., Protat, A., Alexander, S. P., and Berne, A.: Orographic Flow Influence on Precipitation During an Atmospheric River Event at Davis, Antarctica, Journal of Geophysical Research: Atmospheres, 127, e2021JD035 210, https://doi.org/10.1029/2021JD035210, 2022.

https://doi.org/10.5194/egusphere-2026-2155
Preprint. Discussion started: 30 April 2026

Geldenhuys, M., Preusse, P., Krisch, I., Zülicke, C., Ungermann, J., Ern, M., Friedl-Vallon, F., and Riese, M.: Orographically induced spontaneous imbalance within the jet causing a large-scale gravity wave event, Atmospheric Chemistry and Physics, 21, 10 393–10 412, https://doi.org/10.5194/acp-21-10393-2021, 2021.

Giongo, G. A., Bageston, J. V., Figueiredo, C. A. O. B., Wrasse, C. M., Kam, H., Kim, Y. H., and Schuch, N. J.: Gravity Wave Investigations over Comandante Ferraz Antarctic Station in 2017: General Characteristics, Wind Filtering and Case Study, Atmosphere, 11, https://doi.org/10.3390/atmos11080880, 2020.

Grazioli, J., Madeleine, J.-B., Gallée, H., Forbes, R. M., Genthon, C., Krinner, G., and Berne, A.: Katabatic winds diminish precipitation contribution to the Antarctic ice mass balance, Proceedings of the National Academy of Sciences, 114, 10 858–10 863, https://doi.org/10.1073/pnas.1707633114, 2017.

Gumley, L., Descloitres, J., and Schmaltz, J.: Creating reprojected true color MODIS images: A tutorial, University of Wisconsin–Madison, 19, 2003.

Gupta, A., Birner, T., Dörnbrack, A., and Polichtchouk, I.: Importance of Gravity Wave Forcing for Springtime Southern Polar Vortex Breakdown as Revealed by ERA5, Geophysical Research Letters, 48, e2021GL092 762, https://doi.org/10.1029/2021GL092762, 2021.

Gupta, A., Sheshadri, A., Alexander, M. J., and Birner, T.: Insights on Lateral Gravity Wave Propagation in the Extratropical Stratosphere From 44 Years of ERA5 Data, Geophysical Research Letters, 51, e2024GL108 541, https://doi.org/10.1029/2024GL108541, 2024.

Hersbach, H., Bell, B., Berrisford, P., Hirahara, S., Horányi, A., Muñoz-Sabater, J., Nicolas, J., Peubey, C., Radu, R., Schepers, D., Simmons, A., Soci, C., Abdalla, S., Abellan, X., Balsamo, G., Bechtold, P., Biavati, G., Bidlot, J., Bonavita, M., De Chiara, G., Dahlgren, P., Dee, D., Diamantakis, M., Dragani, R., Flemming, J., Forbes, R., Fuentes, M., Geer, A., Haimberger, L., Healy, S., Hogan, R. J., Hólm, E., Janisková, M., Keeley, S., Laloyaux, P., Lopez, P., Lupu, C., Radnoti, G., de Rosnay, P., Rozum, I., Vamborg, F., Villaume, S., and Thépaut, J.-N.: The ERA5 global reanalysis, Quarterly Journal of the Royal Meteorological Society, 146, 1999–2049, https://doi.org/10.1002/qj.3803, 2020.

Hines, C. O.: Generation of Turbulence by Atmospheric Gravity Waves, Journal of Atmospheric Sciences, 45, 1269 – 1278, https://doi.org/10.1175/1520-0469(1988)045<1269:GOTBAG>2.0.CO;2, 1988.

Hocke, K. and Wang, W.: Influence of the Moon phase on ionospheric total electron content observed by GNSS remote sensing, Journal of Space Weather and Space Climate, 15, 35, 2025.

Hoskins, B. J. and Hodges, K. I.: A new perspective on Southern Hemisphere storm tracks, Journal of Climate, 18, 4108–4129, https://doi.org/10.1175/jcli3570.1, 2005.

Hu, Y., Winker, D., Vaughan, M., Lin, B., Omar, A., Trepte, C., Flittner, D., Yang, P., Nasiri, S. L., Baum, B., Holz, R., Sun, W., Liu, Z., Wang, Z., Young, S., Stamnes, K., Huang, J., and Kuehn, R.: CALIPSO/CALIOP Cloud Phase Discrimination Algorithm, Journal of Atmospheric and Oceanic Technology, 26, 2293 – 2309, https://doi.org/10.1175/2009JTECHA1280.1, 2009.

Irving, D., Simmonds, I., and Keay, K.: Mesoscale Cyclone Activity over the Ice-Free Southern Ocean: 1999–2008, Journal of Climate, 23, 5404 – 5420, https://doi.org/10.1175/2010JCLI3628.1, 2010.

Jensen, E. J., Ueyama, R., Pfister, L., Bui, T. V., Alexander, M. J., Podglajen, A., Hertzog, A., Woods, S., Lawson, R. P., Kim, J.-E., and Schoeberl, M. R.: High-frequency gravity waves and homogeneous ice nucleation in tropical tropopause layer cirrus, Geophysical Research Letters, 43, 6629–6635, https://doi.org/10.1002/2016GL069426, 2016.

Jia, M., Yuan, J., Wang, C., Xia, H., Wu, Y., Zhao, L., Wei, T., Wu, J., Wang, L., Gu, S.-Y., Liu, L., Lu, D., Chen, R., Xue, X., and Dou, X.: Long-lived high-frequency gravity waves in the atmospheric boundary layer: observations and simulations, Atmospheric Chemistry and Physics, 19, 15 431–15 446, https://doi.org/10.5194/acp-19-15431-2019, 2019.

https://doi.org/10.5194/egusphere-2026-2155
Preprint. Discussion started: 30 April 2026

Kalesse, H. and Kollias, P.: Climatology of High Cloud Dynamics Using Profiling ARM Doppler Radar Observations, Journal of Climate, 26, 6340 – 6359, https://doi.org/10.1175/JCLI-D-12-00695.1, 2013.

Kalesse-Los, H., Kötsche, A., Foth, A., Röttenbacher, J., Vogl, T., and Witthuhn, J.: The Virga-Sniffer – a new tool to identify precipitation evaporation using ground-based remote-sensing observations, Atmospheric Measurement Techniques, 16, 1683–1704, https://doi.org/10.5194/amt-16-1683-2023, 2023.

Kidston, J., Scaife, A. A., Hardiman, S. C., Mitchell, D. M., Butchart, N., Baldwin, M. P., and Gray, L. J.: Stratospheric influence on tropospheric jet streams, storm tracks and surface weather, Nature Geoscience, 8, 433–440, 2015.

Kollias, P., Puigdomènech Treserras, B., and Protat, A.: Calibration of the 2007–2017 record of Atmospheric Radiation Measurements cloud radar observations using CloudSat, Atmospheric Measurement Techniques, 12, 4949–4964, https://doi.org/10.5194/amt-12-4949-2019, 2019.

Lamer, K., Oue, M., Battaglia, A., Roy, R. J., Cooper, K. B., Dhillon, R., and Kollias, P.: Multifrequency radar observations of clouds and precipitation including the G-band, Atmospheric Measurement Techniques, 14, 3615–3629, https://doi.org/10.5194/amt-14-3615-2021, 2021.

Mace, G. G., Protat, A., Humphries, R. S., Alexander, S. P., McRobert, I. M., Ward, J., Selleck, P., Keywood, M., and McFarquhar, G. M.: Southern Ocean Cloud Properties Derived From CAPRICORN and MARCUS Data, Journal of Geophysical Research: Atmospheres, 126, e2020JD033 368, https://doi.org/10.1029/2020JD033368, 2021.

McDonald, A. J.: Gravity wave occurrence statistics derived from paired COSMIC/FORMOSAT3 observations, Journal of Geophysical Research: Atmospheres, 117, https://doi.org/10.1029/2011JD016715, 2012.

McDonald, A. J., George, S. E., and Woollands, R. M.: Can gravity waves significantly impact PSC occurrence in the Antarctic?, Atmospheric Chemistry and Physics, 9, 8825–8840, https://doi.org/10.5194/acp-9-8825-2009, 2009.

McDonald, A. J., Tan, B., and Chu, X.: Role of gravity waves in the spatial and temporal variability of stratospheric temperature measured by COSMIC/FORMOSAT-3 and Rayleigh lidar observations, Journal of Geophysical Research: Atmospheres, 115, https://doi.org/10.1029/2009JD013658, 2010.

McErlich, C., McDonald, A., Renwick, J., and Schuddeboom, A.: An Assessment of Southern Hemisphere Extratropical Cyclones in ERA5 Using WindSat, Journal of Geophysical Research: Atmospheres, 128, e2023JD038 554, https://doi.org/https://doi.org/10.1029/2023JD038554, 2023.

McFarquhar, G. M., Bretherton, C. S., Marchand, R., Protat, A., DeMott, P. J., Alexander, S. P., Roberts, G. C., Twohy, C. H., Toohey, D., Siems, S., Huang, Y., Wood, R., Rauber, R. M., Lasher-Trapp, S., Jensen, J., Stith, J. L., Mace, J., Um, J., Järvinen, E., Schnaiter, M., Gettelman, A., Sanchez, K. J., McCluskey, C. S., Russell, L. M., McCoy, I. L., Atlas, R. L., Bardeen, C. G., Moore, K. A., Hill, T. C. J., Humphries, R. S., Keywood, M. D., Ristovski, Z., Cravigan, L., Schofield, R., Fairall, C., Mallet, M. D., Kreidenweis, S. M., Rainwater, B., D'Alessandro, J., Wang, Y., Wu, W., Saliba, G., Levin, E. J. T., Ding, S., Lang, F., Truong, S. C. H., Wolff, C., Haggerty, J., Harvey, M. J., Klekociuk, A. R., and McDonald, A.: Observations of Clouds, Aerosols, Precipitation, and Surface Radiation over the Southern Ocean: An Overview of CAPRICORN, MARCUS, MICRE, and SOCRATES, Bulletin of the American Meteorological Society, 102, E894 – E928, https://doi.org/10.1175/BAMS-D-20-0132.1, 2021.

Murphy, B. F. and Simmonds, I.: An Analysis of Strong Wind Events Simulated in a GCM near Casey in the Antarctic, Monthly Weather Review, 121, 522 – 534, https://doi.org/10.1175/1520-0493(1993)121<0522:AAOSWE>2.0.CO;2, 1993.

https://doi.org/10.5194/egusphere-2026-2155
Preprint. Discussion started: 30 April 2026

Murphy, D. J., Alexander, S. P., Klekociuk, A. R., Love, P. T., and Vincent, R. A.: Radiosonde observations of gravity waves in the lower stratosphere over Davis, Antarctica, Journal of Geophysical Research: Atmospheres, 119, 11,973–11,996, https://doi.org/10.1002/2014JD022448, 2014.

Noh, Y.-J., Miller, S. D., Heidinger, A. K., Mace, G. G., Protat, A., and Alexander, S. P.: Satellite-Based Detection of Daytime Supercooled Liquid-Topped Mixed-Phase Clouds Over the Southern Ocean Using the Advanced Himawari Imager, Journal of Geophysical Research: Atmospheres, 124, 2677–2701, https://doi.org/10.1029/2018JD029524, 2019.

Nolan, D. S. and Zhang, J. A.: Spiral gravity waves radiating from tropical cyclones, Geophysical Research Letters, 44, 3924–3931, https://doi.org/10.1002/2017GL073572, 2017.

Orr, A., Phillips, T., Webster, S., Elvidge, A., Weeks, M., Hosking, S., and Turner, J.: Met Office Unified Model high-resolution simulations of a strong wind event in Antarctica, Quarterly Journal of the Royal Meteorological Society, 140, 2287–2297, https://doi.org/10.1002/qj.2296, 2014.

Plougonven, R. and Zhang, F.: Internal gravity waves from atmospheric jets and fronts, Reviews of Geophysics, 52, 33–76, https://doi.org/10.1002/2012RG000419, 2014.

Plougonven, R., Hertzog, A., and Guez, L.: Gravity waves over Antarctica and the Southern Ocean: Consistent momentum fluxes in mesoscale simulations and stratospheric balloon observations, Quarterly Journal of the Royal Meteorological Society, 139, 101–118, 2013.

Radenz, M., Bühl, J., Seifert, P., Baars, H., Engelmann, R., Barja González, B., Mamouri, R.-E., Zamorano, F., and Ansmann, A.: Hemispheric contrasts in ice formation in stratiform mixed-phase clouds: disentangling the role of aerosol and dynamics with ground-based remote sensing, Atmospheric Chemistry and Physics, 21, 17 969–17 994, https://doi.org/10.5194/acp-21-17969-2021, 2021.

Schoeberl, M., Dessler, A., Ye, H., Wang, T., Avery, M., and Jensen, E.: The impact of gravity waves and cloud nucleation threshold on stratospheric water and tropical tropospheric cloud fraction, Earth and Space Science, 3, 295–305, https://doi.org/10.1002/2016EA000180, 2016.

Simmonds, I., Keay, K., and Bye, J. A. T.: Identification and Climatology of Southern Hemisphere Mobile Fronts in a Modern Reanalysis, Journal of Climate, 25, 1945 – 1962, https://doi.org/10.1175/JCLI-D-11-00100.1, 2012.

Tansey, E., Marchand, R., Alexander, S. P., Klekociuk, A. R., and Protat, A.: Southern Ocean Low Cloud and Precipitation Phase Observed During the Macquarie Island Cloud and Radiation Experiment (MICRE), Journal of Geophysical Research: Atmospheres, 128, e2023JD039 205, https://doi.org/10.1029/2023JD039205, 2023.

Tomikawa, Y., Nomoto, M., Miura, H., Tsutsumi, M., Nishimura, K., Nakamura, T., Yamagishi, H., Yamanouchi, T., Sato, T., and Sato, K.: Vertical Wind Disturbances during a Strong Wind Event Observed by the PANSY Radar at Syowa Station, Antarctica, Monthly Weather Review, 143, 1804 – 1821, https://doi.org/10.1175/MWR-D-14-00289.1, 2015.

Turner, J., Lachlan-Cope, T. A., Marshall, G. J., Pendlebury, S., and Adams, N.: An extreme wind event at Casey Station, Antarctica, Journal of Geophysical Research: Atmospheres, 106, 7291–7311, https://doi.org/10.1029/2000JD900544, 2001.

Ugolnikov, O. S.: Cross-wave profiles of altitude and particle size of noctilucent clouds in the case of one-dimensional small-scale gravity wave pattern, Journal of Atmospheric and Solar-Terrestrial Physics, 243, 106 024, https://doi.org/10.1016/j.jastp.2023.106024, 2023.

Vignon, É., Picard, G., Durán-Alarcón, C., Alexander, S. P., Gallée, H., and Berne, A.: Gravity Wave Excitation during the Coastal Transition of an Extreme Katabatic Flow in Antarctica, Journal of the Atmospheric Sciences, 77, 1295 – 1312, https://doi.org/10.1175/JAS-D-19-0264.1, 2020.

https://doi.org/10.5194/egusphere-2026-2155
Preprint. Discussion started: 30 April 2026

Vignon, É., Alexander, S. P., DeMott, P. J., Sotiropoulou, G., Gerber, F., Hill, T. C. J., Marchand, R., Nenes, A., and Berne, A.: Challenging and Improving the Simulation of Mid-Level Mixed-Phase Clouds Over the High-Latitude Southern Ocean, Journal of Geophysical Research: Atmospheres, 126, e2020JD033 490, https://doi.org/10.1029/2020JD033490, 2021.

Watanabe, S., Sato, K., and Takahashi, M.: A general circulation model study of the orographic gravity waves over Antarctica excited by katabatic winds, Journal of Geophysical Research: Atmospheres, 111, https://doi.org/10.1029/2005JD006851, 2006.

Wu, D. L. and Jiang, J. H.: MLS observations of atmospheric gravity waves over Antarctica, Journal of Geophysical Research: Atmospheres, 107, ACL 14–1–ACL 14–6, https://doi.org/10.1029/2002JD002390, 2002.

Yoshiki, M. and Sato, K.: A statistical study of gravity waves in the polar regions based on operational radiosonde data, Journal of Geophysical Research: Atmospheres, 105, 17 995–18 011, https://doi.org/10.1029/2000JD900204, 2000.